# Co-evolutions of temperature and monsoonal precipitation patterns from the latest Pleistocene to the mid-Holocene in Japan: Carbonate clumped isotope record of a stalagmite

**Hirokazu Kato** ( h.kato@eps.s.u-tokyo.ac.jp )
The University of Tokyo https://orcid.org/0000-0003-0512-3694
**Taiki Mori**
Chuo Kaihatsu Corporation
**Shota Amekawa**
The University of Tokyo: Tokyo Daigaku
**Chung-Che Wu**
ETH Zurich
**Chuan-Chou Shen**
National Taiwan University
**Akihiro Kano**
The University of Tokyo: Tokyo Daigaku

**Research article**

**Keywords:** Stalagmite paleoclimatology, Carbonate clumped isotope, Oxygen isotope, Paleotemperature, Paleoprecipitation, Latest Pleistocene, Holocene, Heinrich stadial, Hypsithermal, East Asian summer/winter monsoons

**Posted Date:** March 29th, 2022

**DOI:** https://doi.org/10.21203/rs.3.rs-1454058/v1

# Abstract

Quantitative paleotemperature reconstruction is a challenging and important issue in paleoenvironmental studies, for which carbonate clumped isotope ($\Delta_{47}$) thermometry is a promising approach. Here we analyzed $\Delta_{47}$ values from 66 layers of OT02 stalagmite from Ohtaki Cave in central Japan, covering two separate time intervals (2.6–8.8 and 34.8–63.5 ka) to reconstruct terrestrial temperature and meteoric $\delta^{18}O$ records. The average $\Delta_{47}$ temperature of the Holocene portion of this stalagmite was 16.3°C ± 5.6°C and the average of the latest Pleistocene portion was 9.7°C ± 4.6°C. $\Delta_{47}$ thermometry also revealed that the coldest intervals (5°C–10°C) correspond to the Heinrich stadials HSs4–6, and the warmest interval (up to 19.9°C ± 6.0°C) in middle Holocene (approximately 6–5 ka) accompanied by the Hypsithermal climate optimum. We also reconstructed past meteoric $\delta^{18}O$ by subtracting the temperature effect from stalagmite $\delta^{18}O$. Average meteoric $\delta^{18}O$ was − 8.22‰ ± 0.99‰ VSMOW in the Holocene and − 8.81‰ ± 0.84‰ in the latest Pleistocene. Over centennial timescales, meteoric $\delta^{18}O$ was lower during colder periods, such as Heinrich stadials and the cooling event around 7 ka, and higher in warmer periods, such as Hypsithermal warming. These relations indicated synchronicities of terrestrial paleotemperature and paleoprecipitation in our study region. A temperature dependency of total $^{18}O$ fractionation from sea water to precipitation is a likely reason for the negative correlation between temperature and meteoric $\delta^{18}O$. Additionally, East Asian summer monsoon (EASM) brought larger rainfall of high $\delta^{18}O$ during the warm periods, whereas larger snow/rainfall of low $\delta^{18}O$ brought from East Asian winter monsoon (EAWM) in colder periods. $\delta^{18}O$ of OT02 had thus reflected changes in terrestrial temperature and meteoric $\delta^{18}O$, which are both strongly related to EASM and EAWM conflicting in a centennial timescale.


# 1. Introduction

The oxygen isotopic composition of stalagmite calcite ($\delta^{18}O_C$) is a key source of information for terrestrial paleoclimates. Nevertheless, paleoclimatic interpretation of stalagmite $\delta^{18}O_C$ should consider two main controlling factors: the temperature of calcite formation and the oxygen isotopic composition of cave drip water ($\delta^{18}O_W$). It is impossible to determine their relative importance by measuring only stalagmite $\delta^{18}O_C$. The classical interpretation used in stalagmite paleoclimatic studies was that the change in meteoric $\delta^{18}O$ ($\delta^{18}O_{MW}$) is the principal factor controlling stalagmite $\delta^{18}O_C$ and surpasses others such as temperature change. The conventional approach has given a lot of achievement revealing paleoclimatic histories of meteorological conditions, such as monsoon intensities, moisture trajectory, and precipitation seasonality (e.g., Wang et al., 2001; Kato and Yamada, 2016).

The importance of temperature signals was reaffirmed for late Pleistocene to middle Holocene stalagmites from Mie and Gifu Prefectures, central Japan, located at the eastern margin of the East Asian monsoon (EAM) regime (Mori et al., 2018; Fig. 1). These stalagmites exhibit notably smaller amplitudes of variation in $\delta^{18}O_C$ than comparable Chinese cave records; hence, the glacial/interglacial contrast within these stalagmites can be accounted for by a typical warming temperature of 9°C from the last

glacial maximum (LGM) to the mid-Holocene (Mori et al., 2018). This estimated temperature change is comparable with other paleoclimate studies using stalagmites and lake and marine deposits around the Japanese Islands (Nakagawa et al., 2002; Kawahata et al., 2011; Kigoshi et al., 2014; Uemura et al., 2016). Mori et al. (2018) concluded that climate control on $\delta^{18}O_W$ values was insignificant for Japanese caves, perhaps because of their proximity to moisture sources in the Pacific.

Changes in temperature and precipitation both are principal factors influencing terrestrial climate and are intimately connected. To reconstruct their co-evolution, their signals should be divided quantitatively. Recently, it became possible to separate the signals of temperature change in stalagmite $\delta^{18}O_C$ by virtue of advances in various methods to analyze inclusions in stalagmite, i.e., water inclusion and organic contaminants (TEX86 thermometer; e.g., Wassenburg et al., 2021). Another independent approach to estimate paleotemperature is carbonate clumped isotope ($\Delta_{47}$) thermometry (Ghosh et al., 2006; Eiler, 2007). The method has an advantage in its availability because the target substance of the method is carbonate which is the main component of stalagmite. The principle of clumped isotope thermometry is based on the temperature dependency of the observed abundance anomaly of the $^{13}C$-$^{18}O$ bond in carbonate relative to the stochastic abundance calculated using bulk $\delta^{13}C$ and $\delta^{18}O$ values. The abundance anomaly of $^{13}C^{18}O^{16}O$ ($\Delta_{47}$) in $CO_2$ from acid digestion of carbonate minerals is negatively correlated with the temperature of carbonate precipitation (Ghosh et al., 2006; Schauble et al., 2006). Nevertheless, estimating paleotemperature from stalagmite $\Delta_{47}$ values is challenging. $CO_2$ degassing from cave water leads to isotopic disequilibrium in the dissolved inorganic carbon (DIC) pool and thus a lower $\Delta_{47}$ value of carbonate, which yields higher temperatures than predicted (e.g., Guo and Zhou, 2019). The kinetic isotope effects (KIEs) under these conditions have been reported from natural and laboratory speleothem $\Delta_{47}$ results (Affek et al., 2008, 2014; Daëron et al., 2011; Kluge and Affek, 2012; Affek, 2013; Affek and Zaarur, 2014; Kato et al., 2021). In our previous study (Kato et al., 2019), we analyzed $\Delta_{47}$ values of two sample sets: 1) calcites synthesized at different temperatures (2.9°C–61.0°C) and 2) Japanese natural tufa collected by Kawai et al. (2006). Similar to stalagmite settings, $CO_2$ degassing induces calcite precipitation in tufa by increasing its saturation state in stream water (Ford and Pedley, 1996; Kano et al., 2003, 2019; Kawai et al., 2006). The $\Delta_{47}$ values of tufa were lower than those of synthetic calcites. The evaluated temperature offset between the two calibrations was ~ 4°C which is in the same direction as reported in the stalagmite studies referred above (Kato et al., 2019).

In another previous study of us (Kato et al., 2021), we measured $\Delta_{47}$ values of a stalagmite Hiro-1 from Maboroshi Cave in Hiroshima Prefecture, southwestern Japan (Shen et al., 2010; Hori et al., 2013, 2014; Fig. 1). We applied the temperature calibration evaluated from $\Delta_{47}$ values of tufa (Kato et al., 2019) to the $\Delta_{47}$ values of Hiro-1 stalagmite and revealed terrestrial temperature changes after the LGM to the mid-Holocene, except for some layers in which $\Delta_{47}$ and $\delta^{18}O_C$ were significantly disturbed by strong KIE. The $\Delta_{47}$ values of Hiro-1 exhibit an abrupt warming around 6.3–4.9 ka, which likely corresponds to the Hypsithermal event (Wanner et al., 2008), but the record during the corresponding Heinrich stadial 1 (HS1) was unavailable because of strong influences of KIE related to dry cave conditions (Kato et al., 2021).

In this study, we analyzed the $\Delta_{47}$ values of the OT02 stalagmite (2.6–8.8 and 34.8–63.5 ka; Mori et al., 2018) from Ohtaki Cave (Fig. 1) to obtain a longer climatic record in Japan (back to 63 ka), including four periods of Heinrich stadials (HSs) that have yet to be clarified in Japan. Mori et al. (2018) recognized the four times of positive excursions of $\delta^{18}O_{OT02}$ as Heinrich stadials (HSs6–4 including 5.2) by comparing with $\delta^{18}O$ curves of Greenland ice core (NGRIP members, 2004) and that of another stalagmite (KA03 from Kiriana Cave; Mori et al., 2018).

The climatic and hydrological settings are different in the Ohtaki and Maboroshi Caves (Kato et al., 2021), although these regions are on the mainland of Japan (Fig. 1). A major difference between the climatic settings of these caves is the seasonal bias in precipitation amount. The winter rain/snowfall in the Ohtaki Cave region is significantly larger than that in the Maboroshi Cave region. In addition, Ohtaki Cave lies far from the Seto Inland Sea (SIS), which is an important source of moisture for the Maboroshi Cave (Fig. 1). We compare the co-evolutions of terrestrial temperature and precipitation in the Ohtaki Cave region from the latest Pleistocene to the middle Holocene, with results from the Hiro-1 stalagmite (Kato et al., 2021) and other studies that revealed EAM evolutions, such as the record from a Japanese lake (Nakamura et al., 2013) and records from Chinese continental regions (Porter and An, 1995; Wang et al., 2001; Song et al., 2018).

## 2. Study Area And Material

# 2.1 Ohtaki Cave

Ohtaki Cave (35°44'N, 136°59'E; 400 m asl at the entrance) is located in central Gifu Prefecture, Honshu (Fig. 1). As measured at Nagataki (altitude: 430 m asl), a nearby meteorological station, the annual average rainfall over the latest 40 years was 3081 mm. The region is wet year-round: 22.6% in spring (March–May), 36.0% in summer (June–August), 24.6% in autumn (September–November), and 16.8% in winter (December–February). The 40-year mean annual average temperature is 11.5°C, ranging from −0.3°C in January to 23.9°C in August (Fig. 2a).

Ohtaki Cave has a total length of more than 1000 m (Yura, 2011) into the Permian limestone of the Mino Terrane (Kajita et al., 1971). It comprises three cave levels; stalagmites are best developed in the middle level, which is located 110 m underground. The cave has been modified by artificial tunnels for tourists, but the temperature in the cave remains stable at approximately 13.0°C, which is not sensitive to the seasonal change in surface temperature but higher than the annual mean temperature observed in the nearest weather observatory at Nagataki (11.5°C). A larger amount of water seepage during summer likely elevates the cave water temperature throughout the year.

# 2.2 Material

We analyzed a 140-mm-long stalagmite (OT02) collected from the middle level, 200 m from the cave entrance. U-Th ages and $\delta^{18}O$ values from OT02 have been reported by Mori et al. (2018). The age model of OT02 was established on the basis of U-Th ages from 11 horizons using a Bayesian statistical model

(StalAge; Scholz and Hoffman, 2011). A hiatus of 26 kyr (8.8–34.8 ka) was recognized at a discontinuous surface at the 55 mm horizon (Mori et al., 2018). The age ranges of the upper and lower parts are 2.6–8.8 and 34.8–63.5 ka, respectively; however, the age model of the upper portion of OT02 includes a relatively large uncertainty (up to ± 2.5 kyr; Mori et al., 2018). The lower part of OT02 stalagmite records four Heinrich stadials (HSs4–6 including HS5.2).

The $\delta^{18}O_{OT02}$ (VPDB) values range from − 8.2‰ to − 6.3‰ (Fig. 3a; Mori et al., 2018). At 63.5–34.8 ka, the $\delta^{18}O_{OT02}$ generally becomes higher from older to younger layers and displays four millennial-scale events with amplitude of 0.5‰–1‰. The $\delta^{18}O_{OT02}$ values of the Holocene interval (8.8–2.6 ka) mostly fall between − 7‰ and − 8‰; however, a slight positive shift of about 0.5‰ is observed around 6 ka (Fig. 3a). Mori et al. (2018) suggested that the overall trend of $\delta^{18}O_{OT02}$, with a broad positive shift in 63.5–34.8 ka and lower values in the Holocene, is the same as that of seawater $\delta^{18}O$ (Fig. 3b). The positive excursions of $\delta^{18}O_{OT02}$ corresponding to four Heinrich stadials were observed in the U-Th ages of OT02 at − 61.8 ka (HS6), 56.3–55.1 ka (HS5.2), 48.2–44.9 ka (HS5), and 40.9–38.2 ka (HS4). Mori et al. (2018) linked these four durations with terms of HSs found in a KA03 stalagmite (63.5–60.1 ka, 55.9–54.7 ka, 49.4–48.2 ka, and 41.3–39.7 ka), for which the U-Th age model is more precise than the OT02 age model.

# 2.3 Climatic and hydrological settings of Ohtaki and Maboroshi Caves

Two major moisture sources to Japan are the Pacific Ocean and the Japan Sea, from which the East Asian summer and winter monsoons (EASM and EAWM, respectively) bring moisture mainly by warm southerly winds and cold northerly winds, respectively. The climate of Japan is characterized by clear seasonality because the East Asian summer/winter monsoons migrate across the region. Consequently, the precipitation source switches seasonally between the Pacific Ocean in summer and the Japan Sea in winter (Fukui, 1977). On the Pacific side of the central mountains in Japan, including the sites of Ohtaki Cave (OT02) and Maboroshi Cave (Hiro-1), the EASM delivers the majority of the annual precipitation to the Pacific side of Japan. During the winter, the cold and dry EAWM winds acquire moisture from the Tsushima Warm Current, which blows into the Japan Sea. Most moisture from the Japan Sea side is then released as heavy snow and rainfall on the Japan Sea coast, whereas residual moisture generates comparatively short snow and rainfall on the Pacific side. Consequently, higher $\delta^{18}O_{MW}$ values are observed during the warm season, and lower $\delta^{18}O_{MW}$ values are observed during the cold season in several areas in Japan.

Mori et al. (2018) collected 13 samples of cave drip water at stalagmite OT02 from July 2013 to November 2015, as well as 137 separate rain events from November 2013 to September 2015 at Ohgaki City (altitude 10 m), located 60 km southwest from upstream along the major moist trajectory during the EASM season. The $\delta^{18}O_{MW}$ values at Ohgaki show clearer seasonal differences, i.e., higher values from

March to November (− 5.7‰ ± 2.3‰ in amount-weighted average) and lower values from December to February (− 10.8‰ ± 2.1‰; Mori et al., 2018; Fig. 2c). The drip water $\delta^{18}O$ value at Ohtaki (− 8.3‰ on average) is clearly lower than the average $\delta^{18}O_{MW}$ value at Ohgaki (− 6.4‰; Mori et al., 2018). This discrepancy is explained by locations along the dominant path of moisture trajectory and differences in altitude; Ohtaki Cave is further from the Pacific and at a higher altitude (400 m asl) than Ohgaki (10 m asl). Asai et al. (2014) investigated monthly $\delta^{18}O_{MW}$ values at 11 locations on Mt. Ontake (1030–2750 m asl), 45 km east–northeast of Ohtaki Cave, in 2003–2005. The $\delta^{18}O_{MW}$ values in the region were highest in spring (April–May; approximately − 10‰ to − 8‰), lowest in winter (January–February; approximately − 15‰ to − 14‰), and moderate during the summer (Asai et al., 2014). Although the altitudes of these sites (Nagaya, Ohgaki, and Ontake) differ significantly from that of Ohtaki Cave, there is a common trend in that the lowest $\delta^{18}O_{MW}$ values were observed in winter. Since Ohgaki is located upstream of Ohtaki along the major moisture trajectory of the region, the seasonal pattern of $\delta^{18}O_{MW}$ around Ohtaki Cave is likely most similar to that in Ohgaki.

Hori et al. (2009) collected meteoric water at monthly intervals at Nagaya (Okayama Prefecture), located 20 km east of the site of Hiro-1, in 2005–2007. $\delta^{18}O_{MW}$ exhibited higher values from April to October (− 7.1‰ ± 1.4‰ in amount-weighted average) and lower values from November to March (− 9.7‰ ± 1.4‰; Hori et al., 2009; Fig. 2d).

# 3. Method

# 3.1 Carbonate clumped isotope ($\Delta_{47}$)

# 3.1.1 $\Delta_{47}$ measurement and calculation

We collected subsamples for carbonate clumped isotope ($\Delta_{47}$) measurement from 66 layers throughout OT02. To avoid strong disequilibrium effects as much as possible, subsamples were collected from clear layers excluding opaque and muddy horizons presumed to have formed under depressed and/or discontinuous calcite precipitation.

Five milligrams of powdered carbonate were digested by phosphoric acid at 90°C for ~ 5 min and the generated gas was immediately trapped by a stainless-steel tube cooled by liquid nitrogen. Moisture was separated from $CO_2$ gas using a liquid nitrogen and ethanol slush, after which $CO_2$ was introduced to a 30-m-long capillary column (Supel-Q PLOT) with a helium carrier gas. The column was cooled to − 10°C to remove organic contaminants. Purified $CO_2$ was analyzed with a dual inlet mass spectrometer (Finnigan MAT-253) at Kyushu University configured for measurements of masses 44–49 with pressure adjustment to produce an m/z 44 signal of 16 V. The integration time was 30 s. We applied the Pressure Baseline correction of He et al. (2012) with the off-peak measurement of the background intensities of masses 45–49. Each analysis comprised 5–8 acquisitions, with 4.5 off-peak (nine alternate detections;

five times for the reference side and four times for the sample side), 8 on-peak, and 4 off-peak cycles per acquisition.

Further data processing to obtain $\Delta_{47}$ values was performed using Microsoft Excel spreadsheets that first provided $\Delta_{47}$ value *versus* working gas (Oztech; $\delta^{13}C$ = − 3.61‰ VPDB, and $\delta^{18}O$ = 24.90‰ VSMOW). We applied the $^{17}O$ correction of Brand et al. (2010) (with K = 0.01022461, λ = 0.528) to calculate $\Delta_{47}$ values. Each $\Delta_{47}$ value was adjusted on the absolute reference frame of Dennis et al. (2011) and expressed as $\Delta_{47-ARF}$. Raw $\Delta_{47-[EGvsWG]}$ was 1) corrected using the $\delta^{47}$-dependence slope (− 0.000064‰ in $\Delta_{47}$ per 1‰ of $\delta^{47}$; Kato et al., 2019), 2) converted to $\Delta_{47-RF}$ using an empirical transfer function, and 3) converted to $\Delta_{47-ARF}$ by adding the acid fractionation factor of Defliese et al. (2015). We describe $\Delta_{47-ARF}$ simply as $\Delta_{47}$ unless otherwise noted.

$\Delta_{47}$ measurements were performed for four discrete periods from 2018 to 2019. Each subsample was measured once or twice, and repeated measurements of an in-house calcite standard (Hiroshima standard; $\delta^{13}C$ = − 0.47‰, $\delta^{18}O$ = − 5.04‰ and $\Delta_{47}$ = 0.671‰) for 11, 5, 7, and 6 times for each period demonstrated the stability of $\Delta_{47}$ measurements. The standard errors (1 SD) of $\Delta_{47}$ measurements were calculated for each period and were found to be ± 0.006‰–0.009‰ (n = 5–11), corresponding to ± 1.8°C–3.7°C in the OT02 temperature range (Table 1).

## 3.1.2 Temperature calibration for stalagmite $\Delta_{47}$ value

To estimate paleotemperature from $\Delta_{47}$ values of OT02 stalagmite, we applied an experimental (empirical) calibration established from $\Delta_{47}$ values of natural tufa (Eq. 1; Kato et al., 2019).

$$\Delta_{47} = (0.0336 \pm 0.0036) \times 10^6 / T^2 + (0.301 \pm 0.048), \quad (1)$$

where T is absolute temperatures in Kelvins. The $\Delta_{47}$ temperature calibration of tufa (Eq. 1) was applied to the $\Delta_{47}$ values of Hiro-1 stalagmite and successfully yielded the paleotemperature (Kato et al., 2021). We therefore applied the same calibration (Eq. 1) to stalagmite $\Delta_{47}$ to estimate paleotemperature in this study.

## 3.2 Stable oxygen isotope compositions normalized to seawater values

We corrected the stable oxygen isotope compositions of OT02 by removing variations in the marine oxygen isotope following the assumption and method by Mori et al. (2018). Here, we use the $\delta^{18}O_C$ profile ranging from − 8.2‰ to − 6.3‰ which were analyzed from 644 layers (at 0.2 mm intervals) of the OT02 stalagmite (Mori et al., 2018). Stalagmite $\delta^{18}O_C$ changes with drip water $\delta^{18}O$ derived from meteoric $\delta^{18}O$ ($\delta^{18}O_{MW}$). Although the $\delta^{18}O_{MW}$ is determined via various processes, such as evaporation from seawater, moisture transfer, condensation, and precipitation, it must be controlled by the $\delta^{18}O$ of seawater ($\delta^{18}O_{SW}$),

which is the dominant moisture source in the Japanese Islands. The oxygen isotope values of drip water and OT02 ($\delta^{18}O_{OT02}$) were influenced by changes in $\delta^{18}O_{SW}$, according to their hypothesis. We accounted for the influence from $\delta^{18}O_{SW}$ change ($\Delta^{18}O_{SW}$) according to Mori et al. (2018) to correct the $\delta^{18}O_{OT02}$ values for the $\delta^{18}O_{SW}$ change, as follows:

$$\Delta^{18}O_{SW} = (\delta^{18}O_{foram} - 3.26) \times 1/(5.03 - 3.26), \quad (2)$$

where $\delta^{18}O_{foram}$ is the time series from deep Pacific benthic forams reported for the last glacial cycle (150 kyr) by Lisiecki and Stern (2016). Their data, which is standardized for every 500 years, exhibit variations ranging from + 5.03‰ during the LGM to + 3.26‰. Their $\delta^{18}O_{foram}$ represents the fluctuation in deep water $\delta^{18}O_{SW}$, but it differs very slightly from the value of surface water. However, the $\delta^{18}O_{foram}$ reflects the combined signals of $\delta^{18}O_{SW}$ and ocean temperature. Eq. 2 converts $\delta^{18}O_{foram}$ to $\Delta^{18}O_{SW}$ (Fig. 3b) following the assumption that $^{18}O$ enrichment in seawater during the LGM was 1.0‰ ± 0.1‰ (Schrag et al., 1996, 2002; Bintanja and van de Wal, 2008; Shakun et al., 2015). We follow Mori et al. (2018) in defining the residual variation in $\delta^{18}O_{OT02}$ by subtracting the influence from $\delta^{18}O_{SW}$ change ($\Delta^{18}O_{SW}$) as follows:

$$\Delta^{18}O_{OT02-SW} = \delta^{18}O_{OT02} - \Delta^{18}O_{SW} \text{ (in VPDB scale)}. \quad (3)$$

We then assume that residual variation ($\Delta^{18}O_{OT02-SW}$) reflects variations in hydrologic processes (e.g., fractionation from seawater to vapor, amount effect, and continental effect on meteoric $\delta^{18}O$) and signals of deposition temperature (temperature-dependent fractionation between water and calcite).

## 3.3 Paleometeoric $\delta^{18}O$ reconstruction

As mentioned above, stalagmite $\delta^{18}O_C$ value is controlled by the temperature of calcite formation and the $\delta^{18}O_W$ value of water. Using the paleotemperature determined by carbonate clumped isotope and the temperature dependency of isotopic fractionation between calcite and water, past $\delta^{18}O_W$ values can be calculated from the calcite $\delta^{18}O_C$ value. We applied the temperature dependency of $\delta^{18}O$ of Tremaine et al. (2011; Eq. 4) as follows:

$$1000\ln\alpha_{water-calcite} = 16.1\ (10^3 T^{-1}) - 24.6. \quad (4)$$

Eq. 4 was established for cave deposits (Tremaine et al., 2011) and is also consistent with $\delta^{18}O$ variability in Japanese stalagmites studied by Mori et al. (2018) and Kato et al. (2021).

For the present study, we defined two types of the index of past meteoric isotopes, $\delta^{18}O_{MW}$ and $\Delta^{18}O_{MW-SW}$, which were calculated from $\delta^{18}O_{OT02}$ and $\Delta^{18}O_{OT02-SW}$ (defined in Section 3.2) by following equations.

$\delta^{18}O_{MW} = (1000 + \delta^{18}O_{OT02}) / \alpha_{water-calcite} - 1000$ (5)

$\Delta^{18}O_{MW-SW} = (1000 + \Delta^{18}O_{OT02-SW}) / \alpha_{water-calcite} - 1000$. (6)

$\delta^{18}O_{MW}$ principally refers to cave drip water, which is assumed to be almost the average value of meteoric water $\delta^{18}O$. $\Delta^{18}O_{MW-SW}$ refers to the difference between $\delta^{18}O_{MW}$ and $\delta^{18}O_{SW}$; in other words, the total fractionation in the hydrologic circulation process (from seawater to meteoric water) involving changes in climatic factors including the monsoon intensity, moisture trajectory, and the seasonality of precipitation.

# 4. Results

## 4.1 Carbonate clumped isotope ($\Delta_{47}$)

The $\Delta_{47}$ values of 66 layers in OT02 range from 0.670‰ to 0.747‰ (Fig. 3d), corresponding to 1.4°C–28.6°C using Eq. 1 (Table 1). The overall trend of $\Delta_{47}$ variations broadly agrees with trends of $\delta^{18}O_{OT02}$ and $\Delta^{18}O_{OT02-SW}$. Comparatively high $\Delta_{47}$ values (low temperatures) were observed in portions in which higher $\delta^{18}O_{OT02}$ and $\Delta^{18}O_{OT02-SW}$ values were observed.

The average $\Delta_{47}$ temperature of the Holocene portion (16.3°C, 8.8–2.6 ka) is 6.6°C higher than the average of the lower portion (9.7°C, 63.5–34.8 ka). The observed temperature drops corresponding to the HSs are 3°C–5°C. Higher $\Delta_{47}$ temperatures, which presumably correspond to Hypsithermal event (Wanner et al., 2008) were observed during 5.4–3.8 ka (19.9°C ± 6.0°C) after a temporal cooling around 7 ka. Except for the warm period of Hypsithermal, the average $\Delta_{47}$ temperature during the Holocene is 14.1°C ± 4.1°C.

## 4.2 Oxygen isotopes

$\Delta^{18}O_{OT02-SW}$ shows a smaller variation between − 8.3‰ and − 6.7‰. Most values fall between − 7‰ and − 8‰ (Fig. 3c). Although no significant difference was observed between the averaged $\Delta^{18}O_{OT02-SW}$ values of the latest Pleistocene (63.5–34.8 ka) and the Holocene (8.8–2.6 ka), the $\Delta^{18}O_{OT02-SW}$ show a very slight increasing trend from the lower to the upper portions.

## 4.3 $\delta^{18}O_{MW}$ and $\Delta^{18}O_{MW-SW}$

$\delta^{18}O_{MW}$ and $\Delta^{18}O_{MW-SW}$ values vary between − 10.3‰ and − 6.2‰ and − 11.0‰ and − 6.2‰, respectively (Table 1). The variation in $\delta^{18}O_{MW}$ has a smaller fluctuation range than those of $\delta^{18}O_{OT02}$ and $\Delta^{18}O_{OT02-SW}$ (Fig. 4d). The averaged $\delta^{18}O_{MW}$ and $\Delta^{18}O_{MW-SW}$ values of the Holocene (8.8–2.6 ka) portion are higher than those of the latest Pleistocene (63.5–34.8 ka) portion, as is the crosscurrent of $\delta^{18}O_{OT02}$ and $\Delta^{18}O_{OT02-SW}$ values.

# 5. Discussion

## 5.1 Difference in climatic settings of Ohtaki and Maboroshi Caves

A major difference between the climatic settings of Ohtaki Cave (Nagataki) and Maboroshi Cave (Yuki) is a seasonal bias of precipitation amount. In Nagataki, precipitation during the three winter months (December–February) accounts for 16.8% of annual precipitation and yearly variations in winter precipitation are far larger than those in Yuki (Figs. 2c and d). Consequently, the amount ratio of winter and annual precipitation is an important factor controlling the annual average $\delta^{18}O_{MW}$ values at Ohtaki Cave. On the other hand, in Yuki (near Maboroshi Cave), precipitation during the coldest 3 months (December–February) is limited to only 10% of the annual total and the yearly variation is also very limited in these months (Fig. 2d). The precipitation during the warmer 7 months (April–October) accounts for 78% of the annual total, which is more than three times the precipitation in the other 5 months (November–March; 22%). In the region of Maboroshi Cave, the Chugoku Mountains (1729 m asl) obstruct the winter rain/snowfall from the Japan Sea side. It is therefore estimated that the amount ratio of winter and annual precipitation has less importance for the annual average $\delta^{18}O_{MW}$ values at Maboroshi Cave.

The depths of surrounding seas caused another difference in hydrological settings in a millennial scale. The SIS (Fig. 1b) is currently shallow (mostly < 50 m deep) and is an important vapor source for Maboroshi Cave in Hiroshima. However, the SIS was almost exposed during the glacial sea-level low. Because of the absence of this inland sea, moisture was predominantly transported over longer distances from the marine vapor source. Higher $\delta^{18}O_{MW}$ from the SIS was established by the Holocene glacial retreat (Kato et al., 2021). By contrast, the influence of the SIS is negligible for Ohtaki Cave in Gifu prefecture (Fig. 1b).

## 5.2 Discrimination of KIEs and temperature calibration for OT02 $\Delta_{47}$ values

Before paleoclimatic reconstruction, we inspected the reliability of our results as paleoclimatic records. In principle, both calcite $\delta^{18}O$ and $\Delta_{47}$ values depend on temperature; nevertheless, this temperature dependency can be complicated by the KIE due to $CO_2$ degassing from the parent water. It has been suggested that $CO_2$ degassing elevates $\delta^{18}O$ values and lowers $\Delta_{47}$ values of carbonate minerals by incomplete isotopic exchange among water and DIC species (Guo, 2008; Daëron et al., 2011; Kluge and Affek, 2012; Guo and Zhou, 2019) and can generate isotopic offsets (differences between actual and equilibrium values). Some speleothems show a negative correlation between $\delta^{18}O$ offset and $\Delta_{47}$ offset due to the KIE (Daëron et al., 2011; Wainer et al., 2011; Kluge and Affek, 2012; Kluge et al., 2013; Affek et al., 2014). This type of covariation (negative correlation) between $\delta^{18}O$ and $\Delta_{47}$ offsets develops when

KIE fractionation significantly affects $\delta^{18}O$ and $\Delta_{47}$. In such cases, $\Delta_{47}$ temperature is unusable for paleoclimatic reconstruction.

We examined the covariation between $\Delta^{18}O_{OT02}$ and $\Delta_{47}$ values of the OT02 stalagmite to distinguish the influence from KIE. In the OT02 stalagmite, a weak but positive covariation between $\Delta^{18}O_{OT02-SW}$ and $\Delta_{47}$ values expected for equilibrium conditions was noted throughout (Fig. 5a, $r = 0.36$, $n = 78$, $p < 0.01$).

$\Delta^{18}O_{OT02-SW} = 5.05\ \Delta_{47} - 11.15$ ($n = 78$, $R^2 = 0.132$, $p < 0.01$). (7)

The weak correlation can be due to short-term variations in $\delta^{18}O_{MW}$ and KIE strength, and large errors of ± 0.006‰–0.009‰ for $\Delta_{47}$. However, the positive relationship supports the hypothesis that temperature and temperature-dependent changes are the principal factors controlling both the overall trends of $\Delta_{47}$ and $\Delta^{18}O_{OT02-SW}$, and that the signals ($\Delta_{47}$, $\delta^{18}O_{OT02}$, and $\Delta^{18}O_{OT02-SW}$) are not distubed by changes in the strength of KIE disequilibrium.

For the purpose of comparison, in the case of the Hiro-1 stalagmite, the positive covariation was found also in most parts of the stalagmite, supporting the interpretation that both $\Delta_{47}$ and $\delta^{18}O_{Hiro-1}$ changed mainly as a function of temperature (Kato et al., 2021). However, several layers of low growth rate and high $\delta^{13}C$ in Hiro-1 which imply dry conditions and high prior calcite precipitation (PCP) (Hori et al., 2013) exhibited features of the strong influence of KIE disequilibrium: higher $\delta^{18}O$ values and small $\Delta_{47}$ values. In these layers of the Hiro-1 stalagmite, according to our estimate (Kato et al., 2021), the significantly large PCP associated with dry conditions in Maboroshi Cave likely caused lower $\Delta_{63}$ (similar to $\Delta_{47}$, abundance anomaly of $^{63}CO_3^{2-}$) of drip water DIC and lower $\Delta_{47}$ of the Hiro-1 stalagmite, and the KIE was likely further induced by rapid supersaturation and precipitation in the evaporating water film, in which both $\delta^{18}O$ and $\delta^{13}C$ increased (Kato et al., 2021).

The growth rate of the OT02 stalagmite is higher and more stable (around 1–4 μm/yr in the latest Pleistocene portion and 8–9 μm/yr in the Holocene portion) than that of the Hiro-1 stalagmite (less than 0.3 μm/yr in HS1 and up to 3–4 μm/yr in 6.0–6.5 and 16.5–17.0ka; Hori et al., 2013; Kato et al., 2021). Additionally, subsamples for $\Delta_{47}$ measurements were collected from clear layers of OT02 excluding opaque/muddy horizons to avoid the effect of KIE as much as possible, as mentioned in Section 3.1.1. This is likely the reason for absence of strong KIE disequilibrium in the OT02 stalagmite. Therefore, we deduce that temperature is the dominant control on the OT02 $\Delta_{47}$ record and that the relationship is consistent throughout the growth of OT02 from the latest Pleistocene to the middle Holocene. Further, the average $\Delta_{47}$ temperature during the Holocene, except for the Hypsithermal warm period (14.1°C ± 4.1°C), is extremely similar to the current cave temperature of 13.0°C. Therefore, the temperature reconstruction using tufa calibration (Eq. 1; Kato et al., 2019) appears to be successful; as previously described, another calibration by synthetic calcites in Kato et al. (2019) yields about 4°C higher temperatures from the same $\Delta_{47}$ values (Kato et al., 2019).

# 5.3 Terrestrial paleotemperature

We interpret temperature to be the dominant and consistent control on the OT02 $\Delta_{47}$ record, on the basis of the discussion presented in Section 5.2. The $\Delta_{47}$ temperature record from OT02 (Table 1) is also broadly consistent with known climatic stages, such as cooling during HS6 and cooling around HS5.2, warming during the Holocene, and a warming peak around the Hypsithermal event (9 to 6–5 ka; Wanner et al., 2008), although the cooling in HS5 is not so significant comparing to HS6 and HS5.2 and $\Delta_{47}$ temperature show large scatter during HS4 and the warming peak of the Hypthithermal (Fig. 4c). In the period common to the OT02 and Hiro-1 stalagmites (7.7–4.5 ka), the two stalagmites exhibit very similar patterns in $\Delta_{47}$ temperature (Figs. 4c and d); a rapid warming in 7.0–6.0 ka after a temporal cooling of about 5°C at 7.0 ka from around 15°C at 8.0–7.5 ka and a gradual cooling to the cessation of stalagmite growth. Notably, the data plots of OT02 were calibrated to the age of Hiro-1 by the shapes of $\Delta_{47}$ fluctuations with red vertical bars in Fig. 4, considering the larger dating error for OT02 aforementioned. For the same reason, H5.2 cooling is thought to be responsible for the comparatively low $\Delta_{47}$ temperatures observed around 54.8–54.1 ka of OT02 U-Th age. Thus, three distinct and venial cooling intervals of 3°C–5°C are likely linked to HS6, HS5.2, and HS5 (Fig. 4c). Although the averaged $\Delta_{47}$ temperature of the latest Pleistocene portion of OT02 (63–35 ka) is lower than that of the Holocene portion, the $\Delta_{47}$ temperature in warm periods between each Heinrich stadial reached 10°C–15°C, which is as high as the present temperature and the average of the Holocene.

Our $\Delta_{47}$ temperature equation (Eq. 1) was calibrated using the $\Delta_{47}$ values of natural tufa deposited at 5.6°C–16.0°C. The high $\Delta_{47}$ temperatures over 20°C around 5.4–2.9 ka therefore somewhat deviate from the temperature range covered by Eq. 1. Because of the nature of carbonate clumped isotope thermometry, the uncertainty of $\Delta_{47}$ temperatures is greater at higher temperatures, because the $\Delta_{47}$ value exhibits an inverse proportionality to the square of the temperature in Kelvins. Even after considering these larger errors and uncertainties, the average temperature during the period from 5.4 to 3.8 ka (considering the larger dating error for OT02 mentioned above, which likely corresponds to the warm maximum of 6.3–4.9 ka recorded in Hiro-1) is 19.9°C ± 6.0°C and is clearly higher than the present cave temperature of 13°C.

Seasonal temperature variation is currently very limited in the deeper part of Ohtaki Cave, and it is thus likely that the past cave temperature was also stable on seasonal timescales. The high-average $\Delta_{47}$ temperature during the Hypsithermal does not necessarily mean uniform warming of all seasons. In Nagataki (near Ohtaki Cave), the temperature variation tends to be largest in the colder season (November–April) and smaller in the warmer season (May–October; Fig. 6a). The correlation coefficient (R) of annual and monthly temperatures is large in February–May and September–October and smallest in the warmest months (July–August; Fig. 6a). Together, this indicates that summer temperature is not an important control in the determination of annual average temperatures. Variability in annual average temperature is largely dependent on temperature variability in spring and autumn and is also somewhat dependent on winter temperature. Though the assumption cannot be proven by our stalagmite records,

we raise the possibility that the annual average temperature in Nagataki is characterized by the length of the summer (warmer interval) and the winter (colder interval). We presume that the higher cave temperature of 19.9°C ± 6.0°C observed in the 5.4–3.8 ka period of OT02 (corresponding 6.3–4.9 ka of Hiro-1) was induced by longer high summers and shorter winters than at present, accompanied by the warm climate optimum of the Hypsithermal event.

## 5.4 Features in the correlation between $\Delta_{47}$ *versus* $\Delta^{18}O_{OT02-SW}$

A unified regression of $\Delta_{47}$ *versus* $\Delta^{18}O_{OT02-SW}$ was obtained for the OT02 stalagmite from the latest Pleistocene through the middle Holocene (Eq. 7). However, the slope of 5.05 is significantly shallower than that of the theoretical relationship. Where both stalagmite $\delta^{18}O_C$ and $\Delta_{47}$ are solely controlled by depositional temperature (in other words, assuming a constant drip water $\delta^{18}O_W$), the relationship between $\delta^{18}O_C$ and $\Delta_{47}$ can be theoretically calculated. We applied the temperature dependency of $\Delta_{47}$ (Eq. 1) and $\delta^{18}O$ (Eq. 4; Tremaine et al., 2011). The theoretical relationship between $\Delta_{47}$ and $\Delta^{18}O_{stalagmtie-SW}$ is almost linear, with a slope around 70, but is slightly dependent on the $\Delta_{47}$ value (i.e., temperature) (72.5 at $\Delta_{47}$ = 0.69, 68.5 at $\Delta_{47}$ = 0.74).

The temperature dependency of meteoric water $\delta^{18}O_{MW}$ was viewed as a possible cause for the shallower slope. The apparent positive links between local surface air temperature and the meteoric $\delta^{18}O_{MW}$ have been reported globally (Dansgaard, 1964; Rozanski et al., 1993). This relationship can be explained using the renowned Craig-Gordon-type model of isotopic fractionation during water evaporation and the Rayleigh-type fractionation model during water condensation. It appears reasonable that $\delta^{18}O_{MW}$ would be higher in a temperate climate. To evaluate this interpretation, we defined the temperature-dependent fractionation from seawater to meteoric water as $FT_{SW-MW}$ (in ‰) and expressed the relationships between $\Delta_{47}$ and $\Delta^{18}O_{C\ (OT02\ or\ Hiro-1)-SW}$ as shown in Equations 8 and 9:

$$f(\Delta_{47}) = A\Delta_{47} + B = \Delta^{18}O_{C\ (OT02\ or\ Hiro-1)-SW} - FT_{SW-MW} \quad (8)$$

$$dFT_{SW-MW}/dT = -aFT_{SW-MW} = -aT + b, \quad (9)$$

where T is the temperature in °C and $FT_{SW-MW}$ is assumed to be a linear function of temperature. The temperature-dependent coefficient of $FT_{SW-MW}$ is expressed by *a* (‰/°C). The slope A in Eq. 8 increases with the *a* of Eq. 9 and reaches a theoretical slope of $\Delta_{47}$ *versus* $\Delta^{18}O_{stalagmtie-SW}$ (approximately 70) when *a* takes an appropriate value. In the OT02 stalagmite, Slope A reaches the theoretical slope (approximately 70) when $a_{OT02}$ is at 0.18‰/°C for both the Holocene and latest Pleistocene (red line for the Holocene and blue line for the latest Pleistocene).

In the case of the Hiro-1 stalagmite, different regressions of $\Delta_{47}$ *versus* $\Delta^{18}O_{Hiro-1-SW}$ were obtained from three discrete periods, 18.0–16.0, 14.2–12.6, and 7.7–4.9 ka (Fig. 5a, Kato et al., 2021). An especially large difference was noted between regressions in the pre-Holocene and mid-Holocene. Kato et al. (2021) explained this discrepancy in regressions by differences in meteoric water $\delta^{18}O_{MW}$ ($\Delta^{18}O_{MW-SW}$) due to the presence or absence of the SIS (Fig. 1b), which is an important vapor source for Maboroshi Cave in Hiroshima. Higher $\delta^{18}O_{MW}$ from the SIS was established by the Holocene glacial retreat (Kato et al., 2021). By contrast, the influence of the SIS is negligible for Ohtaki Cave in Gifu prefecture (Fig. 1b). This is likely the reason for the unified regression between $\Delta_{47}$ and $\Delta^{18}O_{OT02-SW}$ (Eq. 7) for Ohtaki Cave (Fig. 5a).

There is another characteristic in the regression slopes of Hiro-1 $\Delta_{47}$ *versus* $\Delta^{18}O_{Hiro-1-SW}$ compared to OT02 values. The regression slopes of Hiro-1 are approximately 40 (37.71–44.15; Kato et al., 2021), which are steeper than those of the OT02 stalagmite (Fig. 5a). Figure 5b also shows the calculation results of $a_{Hiro-1}$ (black lines in Fig. 5b; Kato et al., 2021). The differences in these slopes are thought to be the result of distinct temperature dependencies of meteoric $\delta^{18}O_{MW}$ between these two cave sites. In the Hiro-1 stalagmite, Slope A in Eq. 8 reaches the theoretical slope when $a_{Hiro-1}$ is at 0.077‰–0.098‰/°C (black lines in Fig. 5b; Kato et al., 2021), which is smaller than $a_{OT02}$.

# 5.5 Reason for the larger temperature-dependent coefficient of $FT_{SW-MW}$ (*a*) in OT02

We assume that the divergence in *a* values for OT02 and Hiro-1 are ascribed to regional differences in precipitation characteristics. As described in Section 2.3, in both Nagataki (near Ohtaki Cave; Fig. 2c) and Yuki (near Maboroshi Cave; Fig. 2d), higher $\delta^{18}O_{MW}$ values are observed during the warm season, whereas lower $\delta^{18}O_{MW}$ values are observed in the cold season. However, in Nagataki, winter precipitation accounts for a larger proportion of the annual total, and the yearly variation of winter precipitation is far larger than in Yuki (Figs. 2a and b). Hence, the amount ratio of winter/annual precipitations is an important factor influencing the annual average $\delta^{18}O_{MW}$ values at Ohtaki Cave.

The major control of winter precipitation from the Japan Sea side is the strength of the EAWM. Hirose and Fukudome (2006) found a significant correlation ($R^2$ = 0.85) between the average winter precipitation on the Japan Sea side of Honshu and Hokkaido islands in 1907–2006 and the winter monsoon index of Hanawa et al. (1988), which reflects differences in the sea-level pressures between Irkutsk and Nemuro in winter and represents the strength of the EAWM. Hirose and Fukudome (2006) also found that the Japan Sea SST in winter (November–January) exhibited a significant correlation with winter precipitation on the Japan Sea side ($R^2$ = 0.82). This relation occurs because the high SST of the Japan Sea increases evaporation from seawater, which is the supply source of winter snow/rainfall to Japan. In the Northwest Pacific and East Asia, the land–sea thermal contrast is a driving force behind both the EASM and EAWM. As described above, the proportion of winter/summer precipitation is more variable in the Ohtaki region

and the proportion is largely dependent on winter precipitation. Cooling of the land area results in increased winter precipitation and decreased annual average $\delta^{18}O_{MW}$ values in Ohtaki. This is likely the reason for the apparently larger temperature dependency of meteoric water $\delta^{18}O_{MW}$ (*a*; ‰/°C) in the Ohtaki region.

# 5.6 Paleoprecipitation history

In Section 5.3, we raised an assumption that the changes in cave temperature were arising from interactions between the summer and winter seasons. In Japan, summer and winter climates are characterized by the EASM and EAWM winds, respectively (Fukui, 1977). Generally in the Pacific side of Japan except for south-west islands, winter rain/snowfall has a $\delta^{18}O_{MW}$ value lower than summer rainfall with two peaks of $\delta^{18}O_{MW}$ in spring and autumn (Tanoue et al., 2013). This pattern was also observed in Nagataki and typically in Yuki (Figs. 2c and d). Changes in summer and winter durations might therefore affect the precipitation balance between summer and winter which are intimately connected to EASM and EAWM winds, and consequently determine the annual average of $\delta^{18}O_{MW}$ value. Based on this assumption, paleometeoric water should have a lower $\delta^{18}O_{MW}$ value in colder periods and a higher $\delta^{18}O_{MW}$ value in warmer periods. However, the relation between EASM and EAWM is not simple. Previous paleoclimatic studies have indicated numerous relationships between the intensities of EASM and EAWM: an inverse correlation (Xiao et al., 1995; Yancheva et al., 2007; Liu et al., 2009), a positive correlation (Zhang and Lu, 2007), and both positive and inverse correlations depending on the period and timescale concerned (Steinke et al., 2011; Ge et al., 2017). Recently, Yan et al. (2020) presented simulation results to investigate the relationship between time series changes in EASM and EAWM, showing that their intensities are positively correlated at orbital timescale due to seasonal insolation forcing but are negatively correlated over multidecadal to millennial timescales, primarily as a result of internal variability in the Atlantic Meridional Overturning Circulation and its subsequent teleconnection to East Asia via land–sea thermal contrasts.

Focusing on climatic changes at the centennial–millennial timescale, i.e., HSs and Hypsithermal warming, the result of our meteoric water $\delta^{18}O_{MW}$ reconstruction is consistent with the assumption of a lower (higher) $\delta^{18}O_{MW}$ value in colder (warmer) periods (Fig. 4e). The $\Delta^{18}O_{MW-SW}$ value (and accordingly the $\delta^{18}O_{MW}$ value) was lower in colder periods such as HSs and the period of cooling around 7 ka and higher in warmer periods. This is consistent with the assumption in Section 5.3 that the longer summer durations and higher amounts of EASM rainfall caused the average $\delta^{18}O_{MW}$ value in the Hypsithermal warm period. By contrast, it is presumed that EAWM brought a higher amount of snow and rainfall during long winters to Ohtaki Cave during HSs. The Hypsithermal (also known as the Holocene climatic optimum) is a warming period in northern mid to high latitudes (Wanner et al., 2008) that was commonly defined by the peak of EASM rainfall in Chinese continental regions (An et al., 2000). In Chinese continental regions, Heinrich stadials (HSs1–6) were involved in the EAM changes, the weak EASM, and the strong EAWM (Porter and An, 1995; Wang et al., 2001; Song et al., 2018). In comparison with the

results from Chinese continental regions, our estimation results of higher amounts of EASM rainfall in the Hypsithermal warm period and higher amounts of EAWM snow/rainfall during HSs in the Ohtaki region appear credible. Although our results are based on changes in EASM/EAWM durations rather than their strengths, it is realistic to believe that the duration and strength of EASM/EAWM are positively related. The strong and/or long-lasting EAWM in Heinrich stadial results in a dry winter in Chinese continental regions (Porter and An, 1995; Wang et al., 2001; Song et al., 2018). However, EAWM is an important moisture source for Japan in the winter. We presume that the strong and/or long-lasting EAWM would result in a wet winter in the Japan Sea side in HSs. However, only a few prior investigations from Japan have reported terrestrial climatic records in HSs. Nakamura et al. (2013) performed stratigraphic analyses of acoustic records of sediments in Lake Nojiri, the Japan Sea side of central Japan (Fig. 1b) where winter snowfall accounts for approximately 30% of annual precipitation. They revealed lake level fluctuation during the past 45,000 years and found eight sets of rising and falling levels, although their results contain large dating errors of ± 1,000–15,000 years. They also found that peaks of lake level corresponded to cold climate stages such as HSs1–4 and the Younger Dryas. They presumed that lake level rises were caused by increased snowfall from an enhanced winter monsoon (EAWM). Light blue vertical bands in Fig. 4 indicate the periods of peak lake level in Nojiri identified by Nakamura et al. (2013). Unfortunately, the record of Nakamura et al. (2013) does not include older HSs5–6, for which particularly low $\Delta^{18}O_{MW-SW}$ values were reconstructed from OT02 (Fig. 4e). However, the durations of high lake level periods in Nojiri seem to correspond to the periods of colder temperature and lower $\Delta^{18}O_{MW-SW}$ values. Increased precipitation from EAWM was likely also bought into the Ohtaki region and caused a decrease in the annual average of $\Delta^{18}O_{MW-SW}$ during these cold stages.

As described here, changes in the amount ratio of summer and winter precipitations from EASM and EAWM caused the divergence in $\Delta^{18}O_{MW-SW}$ values in the Ohtaki region, although the temperature dependency of the fractionation between seawater and meteoric water (as discussed in Section 5.5) also accounts for the relationship between temperature and $\Delta^{18}O_{MW-SW}$. The relation that lower/higher meteoric $\delta^{18}O_{MW}$ in warmer/colder climate stages is the opposite to the conventional assumption that meteoric $\delta^{18}O_{MW}$ becomes lower/higher in warm–humid/cold–dry climates due to the so-called “amount effect.”

As described in Section 5.1, precipitation from EAWM is minor in the region of Maboroshi Cave. We suggest that a strong EAWM and weak EASM during cold periods caused the dry conditions of Maboroshi Cave, which might have resulted in the interruptions of the growth of Hiro-1 and KIE disturbance of Hiro-1 records (Figs. 4b and d).

# 6. Summary

We analyzed carbonate clumped isotopes ($\Delta_{47}$) of the OT02 stalagmite from Ohtaki Cave for the age intervals of 2.6–8.8 and 34.8–63.5 ka and revealed changes in terrestrial temperature and meteoric $\delta^{18}O$.

The average $\Delta_{47}$ temperature of the Holocene portion (16.3°C, 8.8–2.6 ka) is 6.6°C higher than that of the latest Pleistocene portion (9.7°C, 63.5–34.8 ka). Decrease in $\Delta_{47}$ temperature correspond to HSs and are approximately 3°C–5°C. We presume that higher cave temperatures of 19.9°C ± 6.0°C observed during the middle Holocene (5.4–3.8 ka of OT02) were induced by longer high summers and shorter winters than at present, accompanied by the Hypsithermal warm climate optimum.

We also reconstructed two indices of meteoric oxygen isotopes, $\delta^{18}O_{MW}$ and $\Delta^{18}O_{MW-SW}$, by subtracting the temperature effect from $\delta^{18}O_{OT02}$ and $\Delta^{18}O_{OT02-SW}$. The averaged $\delta^{18}O_{MW}$ and $\Delta^{18}O_{MW-SW}$ values through the Holocene (8.8–2.6 ka) portion are higher than those of the latest Pleistocene (63.5–34.8 ka) portion. Focusing on climatic changes at centennial–millennial timescale, $\Delta^{18}O_{MW-SW}$ values (and accordingly $\delta^{18}O_{MW}$ values) were lower in colder periods, such as HSs and the cooling event around 7 ka, and higher in warmer periods such as the Hypsithermal. These relationships indicate the co-evolution of terrestrial paleotemperature and paleoprecipitation. In Japan, summer and winter climates are characterized by EASM and EAWM winds, respectively. Rainfall from EASM winds has higher $\delta^{18}O_{MW}$ values and rain/snowfall from EAWM winds has lower $\delta^{18}O_{MW}$ values. Increased precipitation brought by EASM has likely increased the average $\delta^{18}O_{MW}$ in warmer periods such as the Hypsithermal, whereas increased precipitation brought by EAWM has decreased the averaged $\delta^{18}O_{MW}$ in colder periods such as HSs. In centennial timescale, the global warming (cooling) is thought to have resulted in prolonged summer (winter) duration in our study regions, rather than changes in the highest/lowest temperatures. Besides, we presume that seasonal precipitation distributions are also affected by global warming/cooling conditions; during periods of global warming, long-lasting EASM brings more precipitation to the Pacific side of Japan. However, long-lasting EAWM brings more rain/snowfall to the Japan Sea side during periods of global cooling.

Hence, we revealed a trend of lower/higher meteoric $\delta^{18}O_{MW}$ in warmer/colder climate stages. This trend is the opposite of that assumed in conventional stalagmite paleoclimate studies, which suggest that meteoric $\delta^{18}O_{MW}$ becomes lower in warm–humid climates due to the “amount effect.” Our results also do not follow previous interpretations that variation in meteoric $\delta^{18}O_{MW}$ values is the dominant controlling factor of stalagmite $\delta^{18}O$ value. In our study regions, major factors determining the average $\delta^{18}O_{MW}$ value are 1) the proportion between summer and winter precipitation and 2) the temperature dependency of the fractionation from seawater to meteoric water. Additionally, 3) seawater $\delta^{18}O_{SW}$ change ($\Delta^{18}O_{SW}$) at orbital scales also influences $\delta^{18}O_{MW}$. These effects occur due to the hydrological setting in Japan in which moisture is brought from surrounding seas. Factor 1 is related to climatic stages on centennial scales, which is also deeply related to terrestrial temperature. Besides these three factors controlling $\delta^{18}O_{MW}$, 4) temperature-dependent fractionation at the time of stalagmite deposition ($FT_{water-stalagmite}$) is an important control on stalagmite $\delta^{18}O_C$. These temperature effects on $\delta^{18}O_{MW}$ and $\delta^{18}O_C$ are, however, in opposite directions and the negative influence of temperature on $\delta^{18}O_C$ ($FT_{water-stalagmite}$) exceeds the

information available for past $\delta^{18}O_{MW}$. This explains the small amplitude of $\delta^{18}O$ change in Japanese stalagmites (Mori et al., 2018; Kato et al., 2021) and has complicated the interpretation of stalagmite $\delta^{18}O_C$ records using only conventional methods of stalagmite climatology depending only on $\delta^{18}O$ analysis.

# Abbreviations

East Asian monsoon (EAM)

last glacial maximum (LGM)

dissolved inorganic carbon (DIC)

kinetic isotope effect (KIE)

Heinrich stadial (HS)

Seto Inland Sea (SIS)

East Asian summer monsoon (EASM)

East Asian winter monsoons (EAWM)

prior calcite precipitation (PCP)

# Declarations

### Availability of data and material

Table 1 contains all of first appearance data in this study.

### Competing interests

The authors declare that they have no competing interest.


### Funding

This study was supported by Grants-in-Aid from the Japan Society for the Promotion of Science [70782019, 20J00843, and 21K18393 for HK, and 16H02235 and 20H00191 for AK] and partially supported by grants from the Science Vanguard Research Program of the Ministry of Science and Technology (MOST) (110-2123-M-002-009), the National Taiwan University (109L8926 to C-CS), the Higher Education Sprout Project of the Ministry of Education (110L901001 and 110L8907), Taiwan ROC for C-CS.

### Authors' contributions

The study was conceptualized, designed, and proposed by HK. The experiment was conducted by HK, TM, AK, C-CW, and C-CS. This study's manuscript was written by HK and AK. The study was supervised by AK and C-CS. The final manuscript was read and approved by the authors.

### Acknowledgment

Weather data and bathymetric data in this study are from the Japan Meteorological Agency (http://www.jma.go.jp) and the NOAA National Geophysical Data Center, 2009: ETOPO1 1 Arc-Minute Global Relief Model (Accessed in July 2021). We thank Yoshihiro Kuwahara and Ryoko Senda (Kyushu University) for supporting the $\Delta_{47}$ analysis. We thank anonymous reviewers for suggestions and edits that largely improved this manuscript.

# References

1. Affek HP (2013) Clumped isotopic equilibrium and the rate of isotope exchange between $CO_2$ and water. Am J Sci 313:309–325
2. Affek HP, Bar-Matthews M, Ayalon A, Matthews A, Eiler JM (2008) Glacial/interglacial temperature variations in Soreq cave speleothems as recorded by "clumped isotope" thermometry. Geochim Cosmochim Acta 72:5351–5360
3. Affek HP, Matthews A, Ayalon A, Bar-Matthews M, Burstyn Y, Zaarur S, Zilberman T (2014) Accounting for kinetic isotope effects in Soreq Cave (Israel) speleothems. Geochim. Cosmochim Acta 143:303–318
4. Affek HP, Zaarur S (2014) Kinetic isotope effect in $CO_2$ degassing: Insight from clumped and oxygen isotopes in laboratory precipitation experiments. Geochim Cosmochim Acta 143:319–330
5. An Z, Porter SC, Kutzbach JE, Xihao W, Suming W, Xiaodong L, Xiaoqiang L, Weijian Z (2000) Asynchronous Holocene optimum of the East Asian monsoon. Quat Sci Rev 19:743–762
6. Asai K, Tsujimura M, Fantong WY (2014) Temporal variation of stable isotope ratios in precipitation on Chubu-mountainous areas: A case study of Mt. Ontake, Japan (in Japanese). J Jpn Assoc Hydrol Sci 44:67–77
7. Bintanja R, van de Wal RSW (2008) North American ice-sheet dynamics and the onset of 100,000-year glacial cycles. Nature 454:869–872
8. Brand WA, Assonov SS, Coplen TB (2010) Correction for the $^{17}O$ interference in $\delta(^{13}C)$ measurements when analyzing $CO_2$ with stable isotope mass spectrometry (IUPAC Technical Report). Pure Appl. Chem. 82, 1719–1733
9. Daëron M, Guo W, Eiler J, Genty D, Blamart D, Boch R, Drysdale R, Maire R, Wainer K, Zanchetta G (2011) $^{13}C^{18}O$ clumping in speleothems: Observations from natural caves and precipitation experiments. Geochim Cosmochim Acta 75:3303–3317

10. Dansgaard W (1964) Stable isotopes in precipitation. Tellus 16:436–468
11. Defliese WF, Hren MT, Lohmann KC (2015) Compositional and temperature effects of phosphoric acid fractionation on $\Delta_{47}$ analysis and implications for discrepant calibrations. Chem Geol 396:51–60
12. Dennis KJ, Affek HP, Passey BH, Schrag DP, Eiler JM (2011) Defining an absolute reference frame for "clumped" isotope studies of $CO_2$. Geochim. Cosmochim Acta 75:7117–7131
13. Eiler JM (2007) "Clumped-isotope" geochemistry—The study of naturally-occurring, multiply-substituted isotopologues. Earth Planet Sci Lett 262:309–327
14. Ford TD, Pedley HM (1996) A review of tufa and travertine deposits of the world. Earth Sci Rev 41:117–175
15. Fukui T (ed) (1977) The Climate of Japan. Elsevier, Amsterdam
16. Ge Q, Xue Z, Yao Z, Zang Z, Chu F (2017) Anti-phase relationship between the East Asian winter monsoon and summer monsoon during the Holocene? J Ocean Uni China 16:175–183
17. Ghosh P, Adkins J, Affek H, Balta B, Guo WF, Schauble EA, Schrag D, Eiler JM (2006) $^{13}C$–$^{18}O$ bonds in carbonate minerals: A new kind of paleothermometer. Geochim Cosmochim Acta 70:1439–1456
18. Guo W (2008) Carbonate clumped isotope thermometry: Application to carbonaceous chondrites and effects of kinetic isotope fractionation. Ph.D. thesis, Caltech
19. Guo W, Zhou C (2019) Patterns and controls of disequilibrium isotope effects in speleothems: Insights from an isotope-enabled diffusion-reaction model and implications for quantitative thermometry. Geochim Cosmochim Acta 267:196–226
20. Hanawa K, Watanabe T, Iwasaka N, Suga T, Toba Y (1988) Surface thermal conditions in the Western North Pacific during the ENSO events. J Meteorol Soc Jpn 66:445–456
21. He B, Olack GA, Colman AS (2012) Pressure baseline correction and high-precision $CO_2$ clumped-isotope ($\Delta_{47}$) measurements in bellows and micro-volume modes. Rapid Commun Mass Spectrom 26:2837–2853
22. Hirose N, Fukudome K (2006) Monitoring the Tsushima Warm Current improves seasonal prediction of the regional snowfall. SOLA 2:61–63
23. Hori M, Ishikawa T, Nagaishi K, Lin K, Wang B-S, You C-F, Shen C-C, Kano A (2013) Prior calcite precipitation and source mixing process influence Sr/Ca, Ba/Ca and $^{87}Sr/^{86}Sr$ of a stalagmite developed in southwestern Japan during 18.0 4.5 ka. Chem Geol 347:190–198
24. Hori M, Ishikawa T, Nagaishi K, You C-F, Huang K-F, Shen C-C, Kano A (2014) Rare earth elements in a stalagmite from southwestern Japan: A potential proxy for chemical weathering. Geochem J 48:73–84
25. Hori M, Kawai T, Matsuoka J, Kano A (2009) Intra-annual perturbations of stable isotopes in tufas: Effects of hydrological processes. Geochim Cosmochim Acta 73:1684–1695
26. Kajita S, Aoyama S, Kitamura T, Hibino M (1971) The catalogue of limestone caves, Gifu Prefecture, Central Japan 2 (in Japanese). Science report of the Faculty of Education, Gifu University. Nat Sci

4:379–386

27. Kano A, Matsuoka J, Kojo T, Fujii H (2003) Origin of annual laminations in tufa deposits, southwest Japan. Palaeogeogr Palaeoclimatol Palaeoecol 191:243–262
28. Kano A, Okumura T, Takashima C, Shiraishi F (2019) Geobiochenimal Properties of Travertine with Focus on Japanese Sites. Springer, Singapore
29. Kawai T, Kano A, Matsuoka J, Ihara T (2006) Seasonal variation in water chemistry and depositional processes in a tufa-bearing stream in SW-Japan, based on 5 years of monthly observations. Chem Geol 232:33–53
30. Kato H, Amekawa S, Kano A, Mori T, Kuwahara Y, Quade J (2019) Seasonal temperature changes obtained from carbonate clumped isotopes of annually laminated tufas from Japan: Discrepancy between natural and synthetic calcites. Geochim Cosmochim Acta 244:548–564
31. Kato H, Amekawa S, Hori M, Shen C-C, Kuwahara Y, Senda R, Kano A (2021) Influences of temperature and the meteoric water $\delta^{18}O$ value on a stalagmite record in the last deglacial to middle Holocene period from southwestern Japan. Quat Sci Rev 253:106746
32. Kato H, Yamada T (2016) Controlling factors in stalagmite oxygen isotopic composition and the paleoprecipitation record for the last 1,100 years in Northeast Japan. Geochem J 50:e1–e6
33. Kawahata H, Ohshima H, Kuroyanagi A (2011) Terrestrial–Ocean environmental change in the northwestern Pacific from the glacial times to Holocene. J Asian Earth Sci 40:1189–1202
34. Kigoshi T, Kumon F, Hayashi R, Kuriyama M, Yamada K, Takemura K (2014) Climate changes for the past 52 ka clarified by total organic carbon concentrations and pollen composition in Lake Biwa, Japan. Quat Int 333:2–12
35. Kluge T, Affek HP (2012) Quantifying kinetic fractionation in Bunker Cave speleothems using $\Delta_{47}$. Quat. Sci Rev 49:82–94
36. Kluge T, Affek HP, Marx T, Aeschbach-Hertig W, Riechelmann DFC, Scholz D, Riechelmann S, Immenhauser A, Richter DK, Fohlmeister J, Wackerbarth A, Mangini A, Spötl C (2013) Reconstruction of drip-water $\delta^{18}O$ based on calcite oxygen and clumped isotopes of speleothems from Bunker Cave (Germany). Clim Past 9:377–391
37. Lisiecki LE, Stern JV (2016) Regional and global benthic δ18O stacks for the last glacial cycle. Paleoceanography 31:1368–1394
38. Liu X, Dong H, Yang X, Herzschuh U, Zhang E, Stuut J-BW, Wang Y (2009) Late Holocene forcing of the Asian winter and summer monsoon as evidenced by proxy records from the northern Qinghai – Tibetan Plateau. Earth Planet Sci Lett 280:276–284
39. Mori T, Kashiwagi K, Amekawa S, Kato H, Okumura T, Takashima C, Wu C-C, Shen C-C, Quade J, Kano A (2018) Temperature and seawater isotopic controls on two stalagmite records since 83 ka from maritime Japan. Quat Sci Rev 192:47–58
40. Nakagawa T, Tarasov PE, Nishida K, Gotanda K, Yasuda Y (2002) Quantitative pollen-based climate reconstruction in central Japan: Application to surface and Late Quaternary spectra. Quat Sci Rev

21:2099–2113

41. Nakamura Y, Inouchi Y, Inoue T, Kondo Y, Kumon F, Nagahashi Y (2013) Lake-level changes and their factors during the last 45,000 years in Lake Nojiri, Central Japan (in Japanese). Quaternary Res (Daiyonki-Kenkyu) 52:203–212
42. NGRIP members (2004) High-resolution record of Northern Hemisphere climate extending into the last interglacial period. Nature 431:147–151
43. Porter SC, An Z (1995) Correlation between climate events in the North Atlantic and China during the last glaciation. Nature 375:305–308
44. Rozanski K, Araguas-Araguas L, Gonfiantini R (1993) Isotopic Patterns in Modern Global Precipitation. Geophys Monogr 78:1–36
45. Schauble EA, Ghosh P, Eiler JM (2006) Preferential formation of $^{13}C$–$^{18}O$ bonds in carbonate minerals, estimated using first-principles lattice dynamics. Geochim Cosmochim Acta 70:2510–2529
46. Scholz D, Hoffmann DL (2011) StalAge – An algorithm designed for construction of speleothem age models. Quat Geochronol 6:369–382
47. Schrag DP, Adkins JF, McIntyre K, Alexander JL, Hodell DA, Charles CD, McManus JF (2002) The oxygen isotopic composition of seawater during the Last Glacial Maximum. Quat Sci Rev 21:331–342
48. Schrag DP, Hampt G, Murray DW (1996) Pore fluid constraints on the temperature and oxygen isotopic composition of the glacial ocean. Sci 272:1930–1932
49. Shakun JD, Lea DW, Lisiecki LE, Raymo ME (2015) An 800-kyr record of global surface ocean $\delta^{18}O$ and implications for ice volume-temperature coupling. Earth Planet Sci Lett 426:58–68
50. Shen C-C, Kano A, Hori M, Lin K, Chiu T-C, Burr GS (2010) East Asian monsoon evolution and reconciliation of climate records from Japan and Greenland during the last deglaciation. Quat Sci Rev 29:3327–3335
51. Steinke S, Glatz C, Mohtadi M, Groeneveld J, Li Q, Jian Z (2011) Past dynamics of the East Asian monsoon: No inverse behaviour between the summer and winter monsoon during the Holocene. Glob Planet Change 78:170–177
52. Song J-L, Sun H-Y, Tian M-Z, Zhang X-J, Wen X-F, Sun M (2018) Heinrich events recorded in a loessepaleosol sequence from Hexigten, Inner Mongolia. Geosci Front 9:431–439
53. Tanoue M, Ichiyanagi K, Shimada J (2013) Seasonal variation and spatial distribution of stable isotopes in precipitation over Japan (in Japanese). J Jpn Assoc Hydrol Sci 43:73–91
54. Tremaine DM, Froelich PN, Wang Y (2011) Speleothem calcite farmed in situ: Modern calibration of $\delta^{18}O$ and $\delta^{13}C$ paleoclimate proxies in a continuously-monitored natural cave system. Geochim Cosmochim Acta 75:4929–4950
55. Uemura R, Nakamoto M, Asami R, Mishima S, Gibo M, Msaka K, Chen J-P, Wu C-C, Chang Y-W, Shen C-C (2016) Precise oxygen and hydrogen isotope determination in nanoliter quantities of speleothem

inclusion water by cavity ring-down spectroscopic techniques. Geochim Cosmochim Acta 172:159–176

56. Wainer K, Genty D, Blamart D, Daëron M, Bar-Matthews M, Vonhof H, Dublyansky Y, Pons-Branchu E, Thomas L, van Calsteren P, Quinif Y, Caillon N (2011) Speleothem record of the last 180 ka in Villars cave (SW France): Investigation of a large $\delta^{18}O$ shift between MIS6 and MIS5. Quat Sci Rev 30:130–146
57. Wang YJ, Cheng H, Edwards RL, An ZS, Wu JY, Shen C-C, Dorale JA (2001) A high-resolution absolute-dated late pleistocene monsoon record from Hulu Cave. China Sci 451:1090–1093
58. Wanner H, Beer J, Bütikofer J, Crowley TJ, Cubasch U, Flückiger J, Goosse H, Grosjean M, Joos F, Kaplan JO, Küttel M, Müller SA, Prentice IC, Solomina O, Stocker TF, Tarasov P, Wagner M, Widmann M (2008) Mid- to Late Holocene climate change: An overview. Quat Sci Rev 27:1791–1828
59. Wassenburg JA, Vonhof HB, Cheng H, Martínez-García A, Ebner P-R, Li X, Zhang H, Sha L, Tian Y, Edwards RL, Fiebig J, Haug GH (2021) Penultimate deglaciation Asian monsoon response to North Atlantic circulation collapse. Nat Geosci 14:937–941
60. Xiao J, Porter SC, An Z, Kumai H, Yoshikawa S (1995) Grain size of quartz as an indicator of winter monsoon strength on the Loess Plateau of central China during the last 130,000 year. Quat Res 43:22–29
61. Yan M, Liu ZY, Ning L, Liu J (2020) Holocene EASM-EAWM relationship across different timescales in CCSM3.Geophys. Res. Lett.47, e2020GL088451.
62. Yancheva G, Nowaczyk NR, Mingram J, Dulski P, Schettler G, Negendank JFW, Liu J, Sigman DM, Peterson LC, Haug GH (2007) Influence of the intertropical convergence zone on the East Asian monsoon. Nature 445:74–77
63. Yura K (2011) Visit and consideration of Ohtaki Limestone Cave (tourism cave), Gujo City, Gifu Prefecture (in Japanese). Cave Environ NET Soci 2:3–10
64. Zhang D, Lu L (2007) Anti-correlation of summer/winter monsoons? Nature 450:E7–E8

# Table

Tables 1 is available in the Supplementary Files section.

# Figures

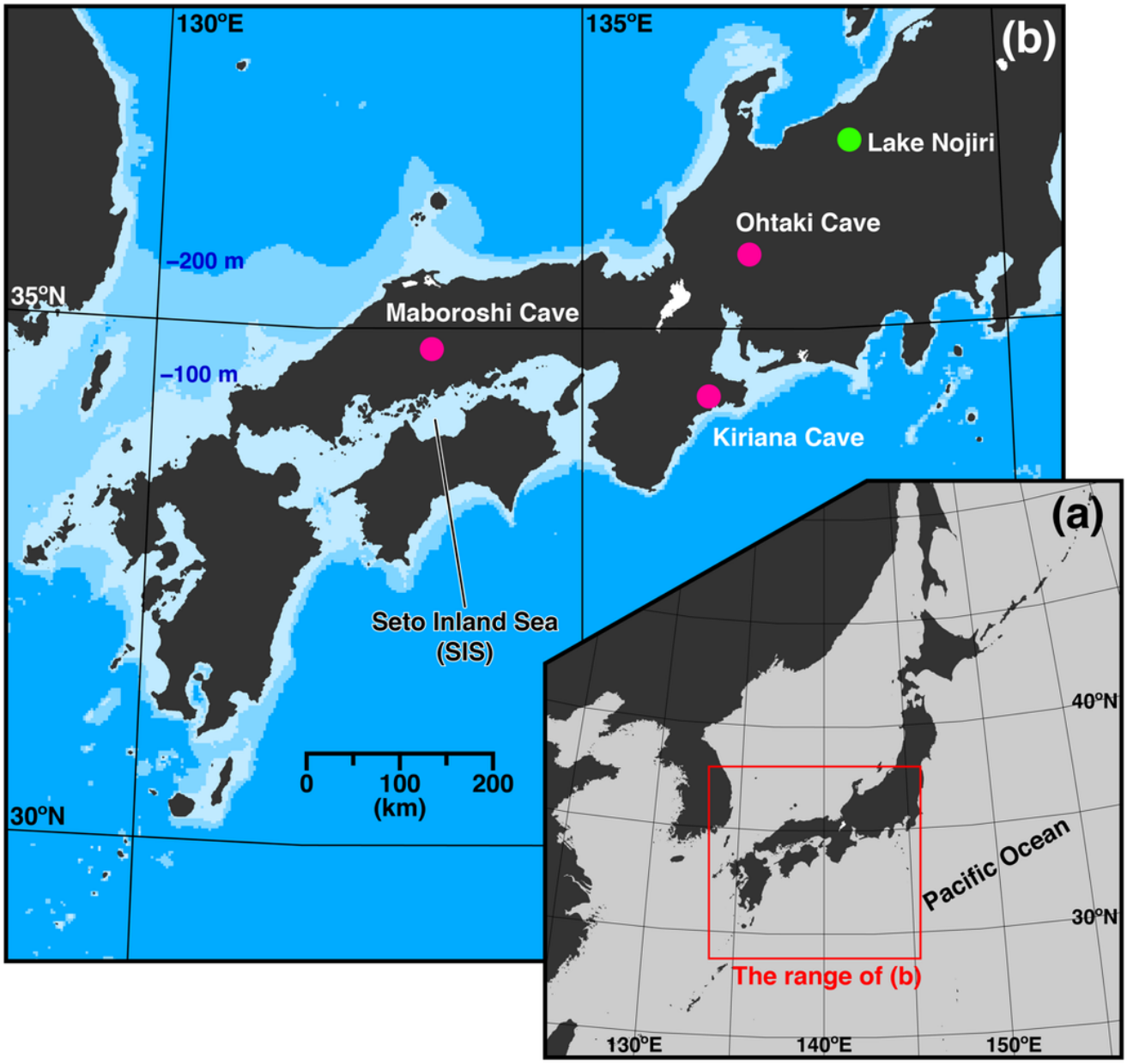


## Figure 1

Maps of study sites. (a) Location of our study area and (b) bathymetric map of western Japan showing the locations of Ohtaki Cave, Maboroshi Cave, Kiriana Cave, and Lake Nojiri.

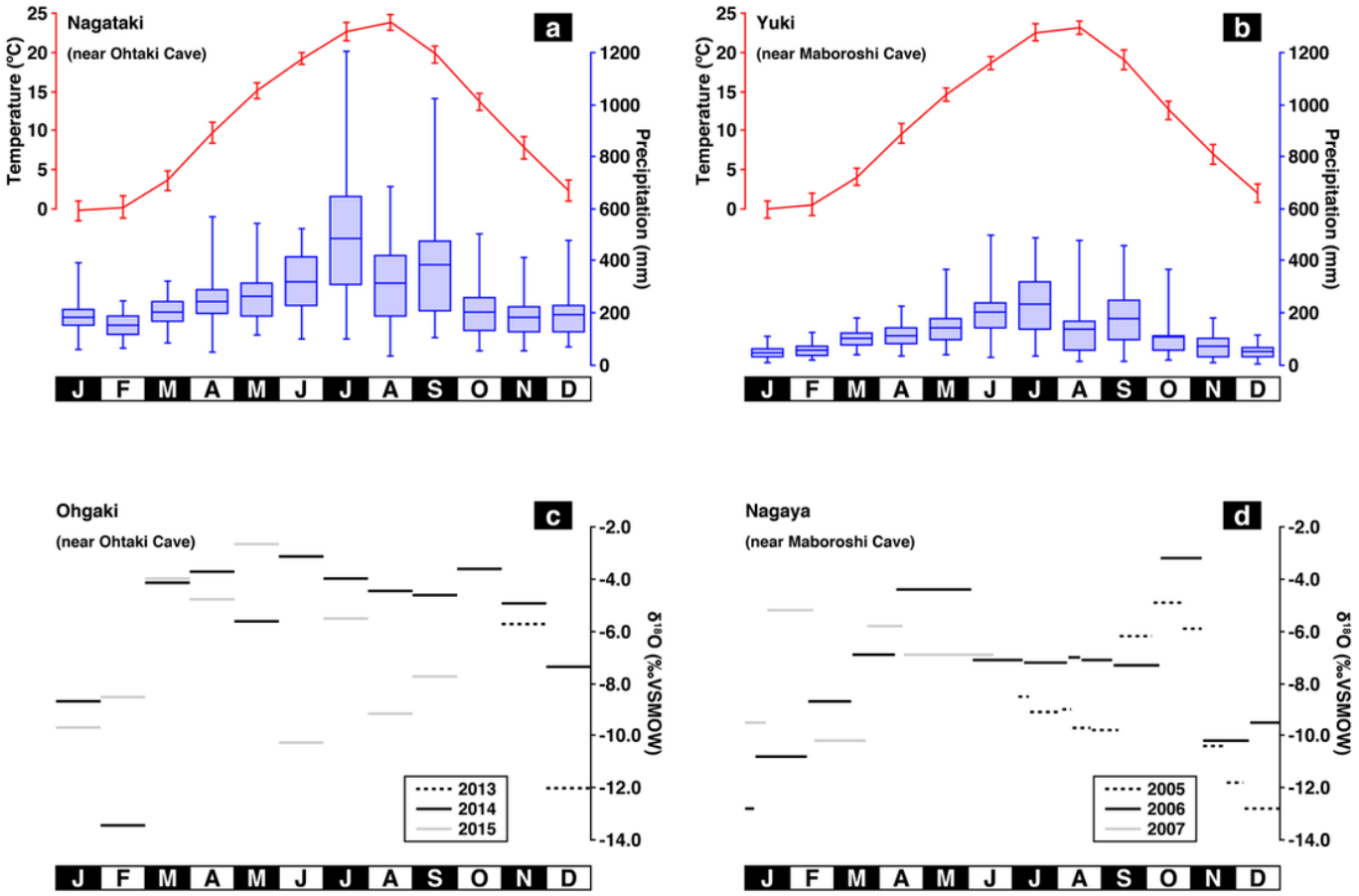


## Figure 2

Climatic conditions at the (a) Nagataki and (b) Yuki observatories over the period 1981–2020 and the oxygen isotopic compositions of meteoric water at (c) Ohgaki and (d) Nagaya. (a, b) Average monthly air temperatures are shown with errors of 1σ. The box plot of precipitation shows the first and third quartiles, and the whisker lengths depict the ranges between the minimum and maximum values. Averaged monthly precipitation is shown by horizontal bars in the boxes. (c, d) Rainwater was collected for each rain event at Ohgaki city, 60 km southwest from Ohtaki Cave, by Mori et al. (2018) and for each month at Nagaya, 20 km east from Maboroshi Cave, by Hori et al. (2009). The bars in (c) show the weighted average values for each month.

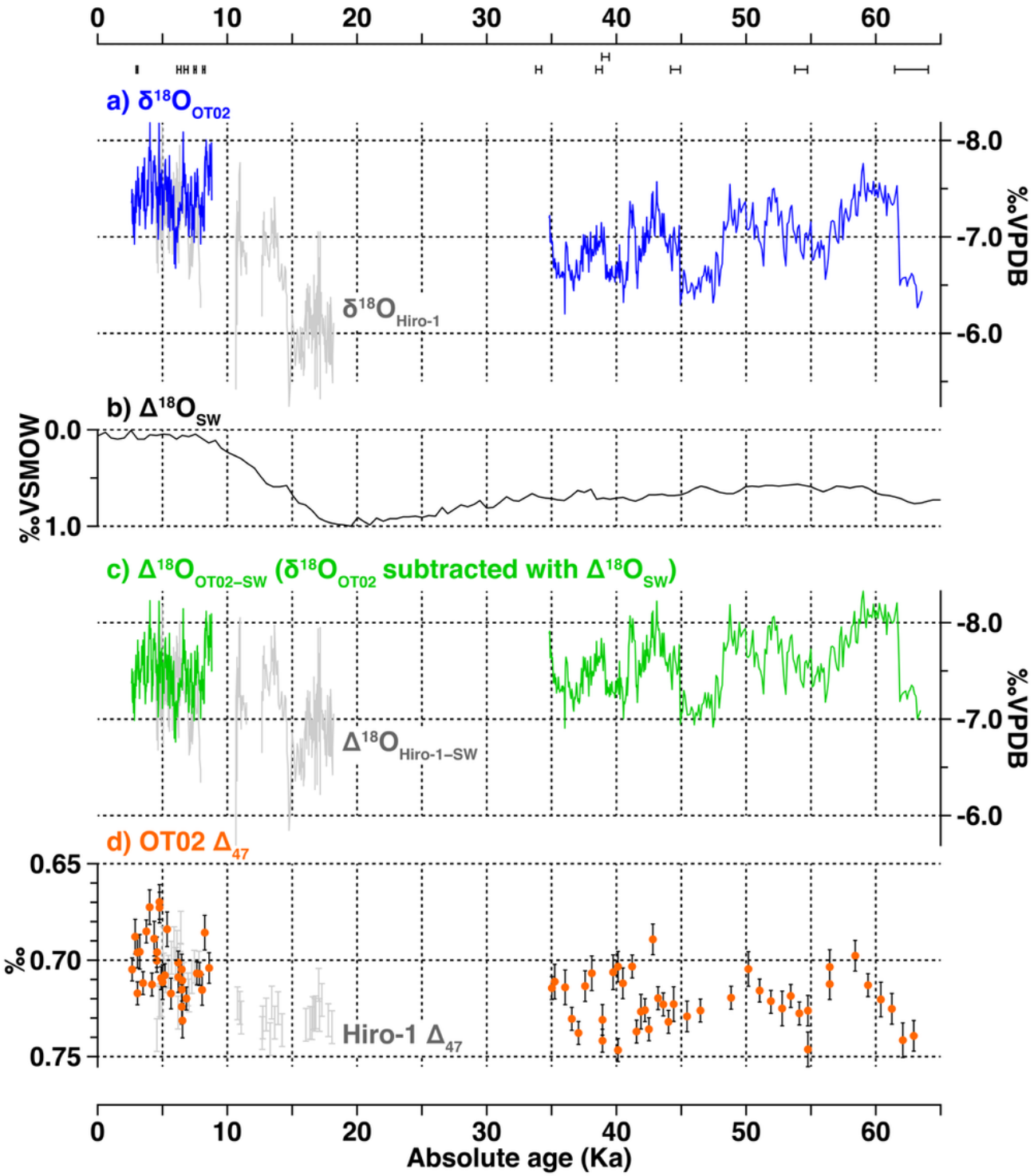


## Figure 3

(a) Time series changes of $\delta^{18}O_{OT02}$ (Mori et al., 2018), (b) $\delta^{18}O_{SW}$ (modified from Lisiecki and Stern, 2016), (c) $\Delta^{18}O_{OT02-SW}$, and (d) $\Delta_{47}$ of OT02. The error bars of $\Delta_{47}$ show the SD of in-house standard measurements (±‰). Data for OT02 (a, c, and d) are shown alongside (a) $\delta^{18}O_{Hiro-1}$, (c) $\Delta^{18}O_{Hiro-1-SW}$, and $\Delta_{47}$ of Hiro-1 (Hori et al., 2013; Kato et al., 2021) as gray lines and bars.

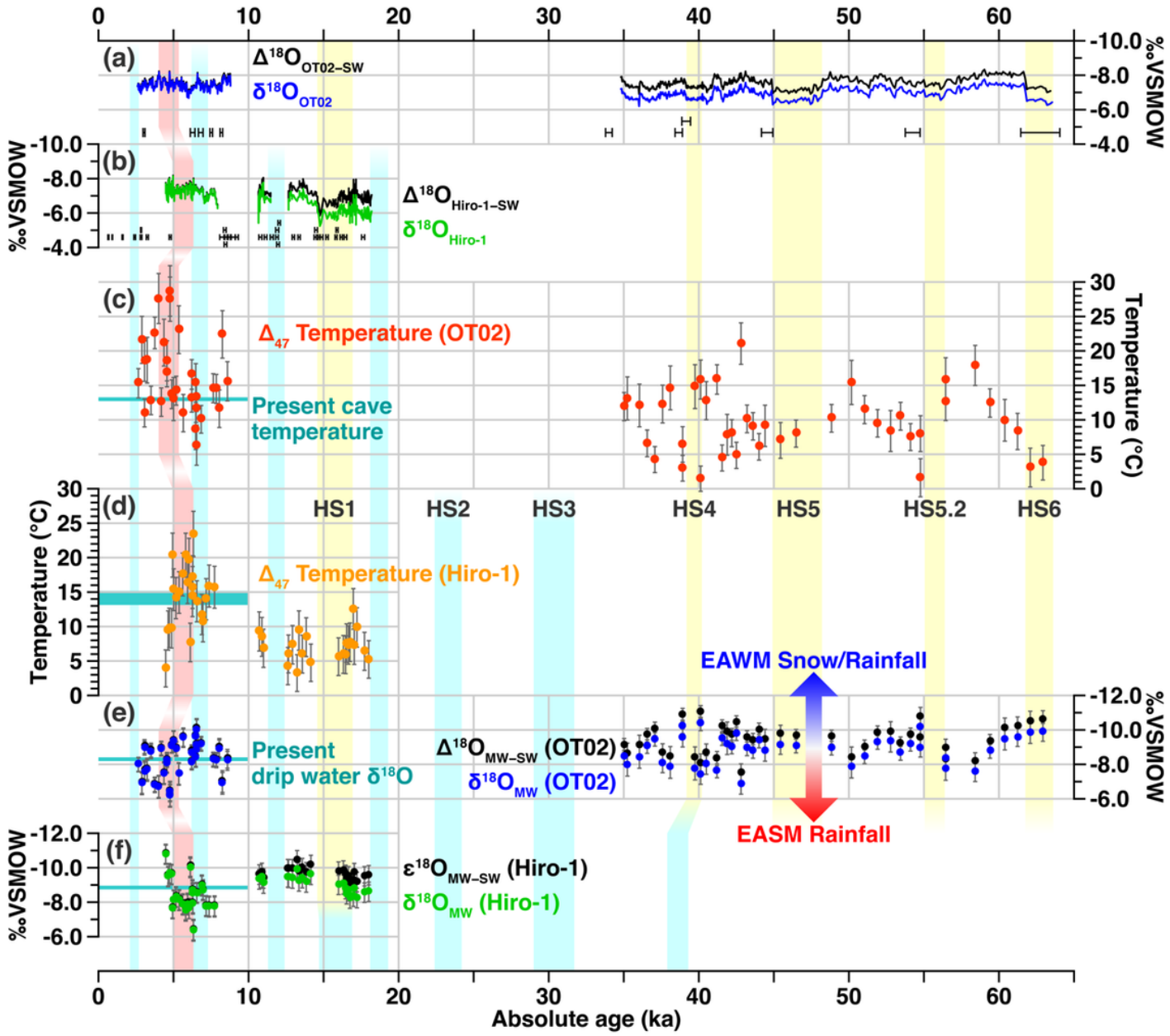


## Figure 4

(c) $\Delta_{47}$ temperature, (e) $\delta^{18}O_{MW}$ and $\Delta^{18}O_{MW-SW}$ from the OT02 stalagmite compared with (d, f) the results of the Hiro-1 stalagmite (Kato et al., 2021). The values of $\delta^{18}O_{MW}$ and $\Delta^{18}O_{MW-SW}$ for (e) OT02 and (f) Hiro-1 were calculated from (a) $\delta^{18}O_{OT02}$ and $\Delta^{18}O_{OT02-SW}$ and (b) $\delta^{18}O_{Hiro-1}$ and $\Delta^{18}O_{Hiro-1-SW}$, respectively, by the subtraction of temperature effect (Eqs. 5 and 6) using (c, d) $\Delta_{47}$ temperatures. Yellow-vertical bands show the periods of Heinrich stadials. Light-blue bands show the periods of high lake level in Lake Nojiri, which occurs after heavy snowfall from EAWM as shown by Nakamura et al. (2013). The light-red band shows a period of warm climatic optimum corresponding to the Hypsithermal observed both in this study and in the Hiro-1 stalagmite of Kato et al. (2021).

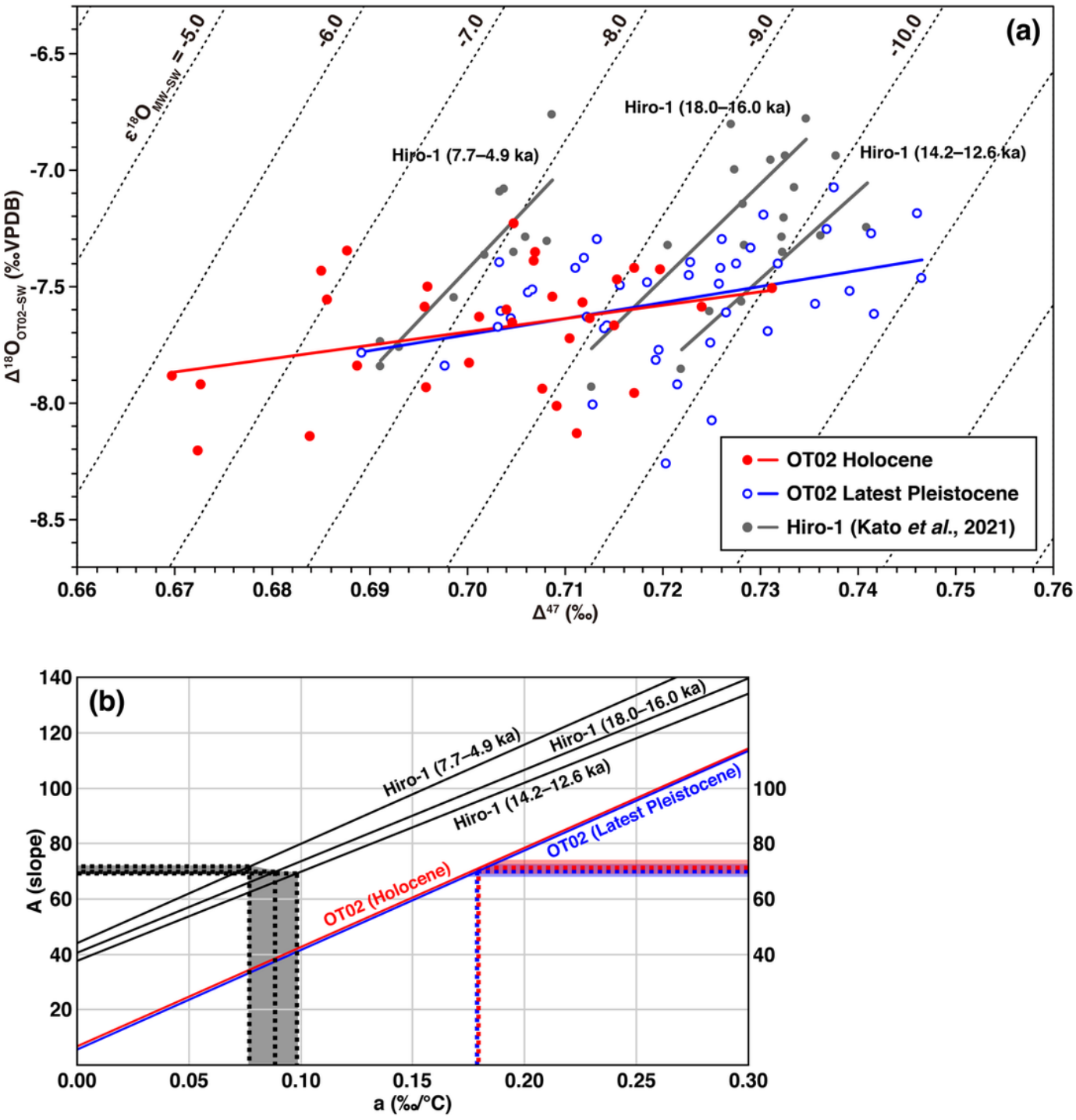


## Figure 5

(a) Cross-plot of OT02 $\Delta_{47}$ and $\Delta^{18}O_{OT02-SW}$. Dashed lines show the theoretical relationships at stable $\Delta^{18}O_{MW-SW}$ values from −13.0‰ to −4.0‰ (VSMOW) calculated using Equations 3 and 4 (Kato et al., 2019; Tremaine et al., 2011).

The regression lines of OT02 are given for the Holocene (in red) and latest Pleistocene (in blue) and they are indistinguishable from each other. The slopes of these lines are clearly shallower than the theoretical relationships and the three discrete regression lines for the Hiro-1 stalagmite (Kato et al., 2021). (b) Slopes of regression lines (A in Eq. 6) between $\Delta_{47}$ and ($\Delta^{18}O_{OT02-SW}$ – $FT_{SW-MW}$) under the variable temperature dependency of $FT_{SW-MW}$ (*a* in Eq. 7). The *a* value for OT02 is 0.18 (‰/°C), which is clearly larger than that for Hiro-1, 0.08–0.10 (‰/°C; Kato et al., 2021).

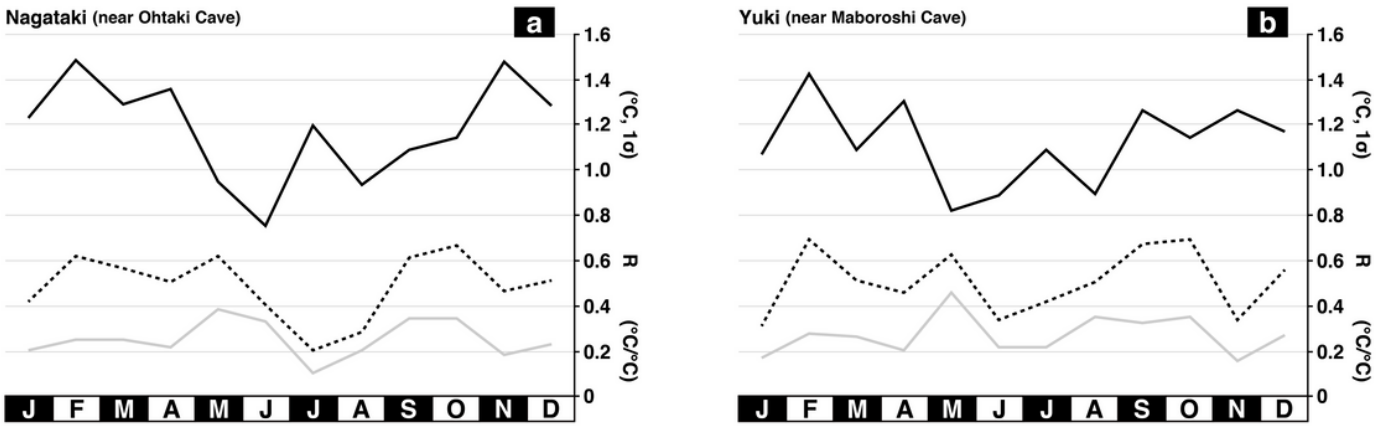


**Figure 6**

Relationship between monthly and annual mean temperatures in (a) Nagataki and (b) Yuki based on data for the period 1981–2020. Black lines show standard deviations in monthly mean temperature (1σ). Dashed lines show the correlation coefficient (R) between monthly and annual mean temperatures. Gray lines show the impacts of monthly temperatures on the annual average (°C /°C).

# Supplementary Files

This is a list of supplementary files associated with this preprint. Click to download.

- Table1.xlsx
- OT02graphicalabstractrev.pdf